Current Biology 22, 269–277, February 21, 2012 ©2012 Elsevier Ltd All rights reserved DOI 10.1016/j.cub.2012.01.011

Article

Functional Biases in Visual Cortex Neurons with Identified Projections to Higher Cortical Targets

Beata Jarosiewicz,[1,5,*] James Schummers,[1,6] Wasim Q. Malik,[2,4] Emery N. Brown,[2,3,4] and Mriganka Sur[1,2,*]
[1]Picower Institute for Learning and Memory
[2]Department of Brain and Cognitive Sciences
[3]Division of Health Sciences and Technology
Massachusetts Institute of Technology, Cambridge, MA 02139, USA
[4]Department of Anesthesia, Critical Care and Pain Medicine, Massachusetts General Hospital, Harvard Medical School, Boston, MA 02114, USA

Summary

Background: Visual perception involves information flow from lower- to higher-order cortical areas, which are known to process different kinds of information. How does this functional specialization arise? As a step toward addressing this question, we combined fluorescent retrograde tracing with in vivo two-photon calcium imaging to simultaneously compare the tuning properties of neighboring neurons in areas 17 and 18 of ferret visual cortex that have different higher cortical projection targets.
Results: Neurons projecting to the posterior suprasylvian sulcus (PSS) were more direction selective and preferred shorter stimuli, higher spatial frequencies, and higher temporal frequencies than neurons projecting to area 21, anticipating key differences between the functional properties of the target areas themselves. These differences could not be explained by a correspondence between anatomical and functional clustering within early visual cortex, and the largest differences were in properties generated within early visual cortex (direction selectivity and length preference) rather than in properties present in its retinogeniculate inputs.
Conclusions: These projection cell groups, and hence the higher-order visual areas to which they project, likely obtain their functional properties not from biased retinogeniculate inputs but from highly specific circuitry within the cortex.

Introduction

Modular functional organization is a fundamental principle of cortical processing [1]. In primates, more than 30 specialized visual cortical regions are recognized, and they are organized into a loose hierarchy of ascending receptive field size and complexity [2–4]. In other species, such as carnivores, a number of homologous cortical areas have been described, and similar organization principles appear to hold [5, 6]. At the first stage of visual cortical processing, it is thought that functional specialization such as orientation selectivity arises through a combination of biased inputs arriving from thalamus [7] and elaboration and refinement of these biases by intracortical connectivity [8, 9].

Whether similar principles underlie the generation of functional specialization in higher cortical areas remains unknown. As a step toward addressing this issue, we have developed a method to test whether functional biases exist in the response properties of neurons in a lower-order cortical area that project differentially to either of two higher-order cortical areas downstream. By combining dual retrograde fluorescent labeling, which allows cells with distinct projection targets to be visualized in distinct colors, with in vivo two-photon calcium imaging, which makes it possible to characterize the tuning properties of those retrogradely labeled cells, we were able to directly compare the tuning properties of these two sets of projection neurons in primary visual cortex simultaneously and at single-cell resolution.

Of several high-order visual cortical areas that have been described in carnivores, we focused on two areas that receive direct projections from primary visual cortex and are at similar, intermediate stages of the visual processing hierarchy in the ferret, posterior suprasylvian sulcus (PSS) and area 21. PSS of ferrets is homologous to the posteromedial lateral suprasylvian area (PMLS) of cats [10–12] and is therefore a likely analog of monkey medial temporal cortex (MT) [5, 6, 13]; cells in PSS and PMLS are highly direction selective, show strong end suppression (i.e., the extension of stimuli outside of their receptive field centers inhibits their activity), and prefer high temporal frequencies [14–16]. Area 21 of ferrets is homologous to area 21a of cats [15, 17–19] and is therefore a likely analog of monkey V4 [6]; cells here are less direction selective, show length summation rather than length suppression (i.e., their responses increase monotonically with bar length), and prefer lower temporal frequencies [16, 20, 21]. We found that these differences in receptive field characteristics in PSS and area 21 are foreshadowed by biases in the tuning properties of spatially interleaved visual cortical neurons that project differentially to these two areas, supporting the hypothesis that the principles underlying the generation of functional specialization in higher-order cortical areas are similar to those that have been proposed for lower-order areas.

Results

To identify those neurons in early visual cortex that project to PSS versus to area 21, we injected a retrograde tracer (cholera toxin B, or CTB) conjugated to one of two different fluorescent markers (Alexa Fluor 555 or 594), one into area PSS and the other into area 21 of ferret visual cortex (see Experimental Procedures; see also Supplemental Experimental Procedures and Figure S1 available online). Injections were made at matched cortical locations representing similar, central locations of the visual field [19]. After neurons were retrogradely filled (5–12 days after the injection; see Table S1), we implanted a cranial window over posterior visual cortex, bulk loaded a region of either area 17 or area 18 containing both sets of retrogradely filled cells with the calcium indicator dye Oregon green 488-BAPTA, and characterized their activity in response to visual stimuli using in vivo two-photon imaging (Figure 1).

As expected from the anatomy of feedforward projections in cat visual cortex [22, 23], most of the retrogradely labeled cells

[5]Present address: Department of Neuroscience, Brown University, Providence, RI 02912, USA
[6]Present address: Max Planck Florida Institute, Jupiter, FL 33468, USA
*Correspondence: jarosiew@gmail.com (B.J.), msur@mit.edu (M.S.)

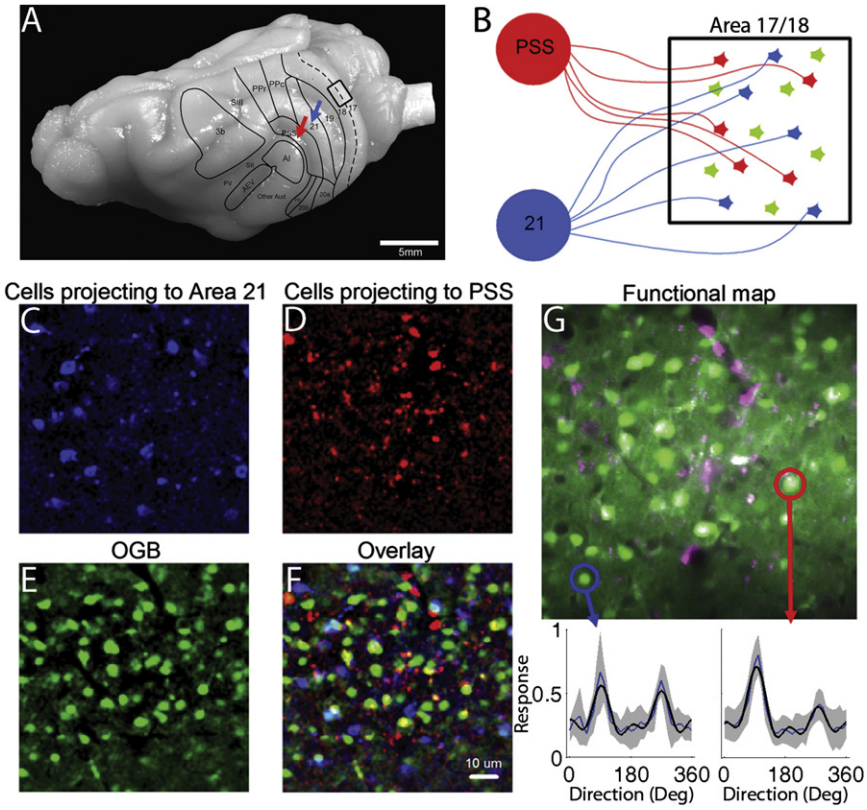

Figure 1. Labeling and Imaging Area 17/18 Cells that Project to Distinct Cortical Targets

(A) Location of visual areas in the ferret cortex (modified with permission from [51]). Injections of retrograde tracers CTB-594 and CTB-555 were made into PSS (red arrow) and area 21 (blue arrow) to label projection neurons in areas 17 and 18.

(B) Distinct sets of projection neurons in area 17/18 projecting to area 21 (blue) or PSS (red) could then be identified and bulk loaded with the calcium indicator dye Oregon green 488-BAPTA (OGB), allowing their physiological response features to be characterized.

(C–F) Example of an imaging region in area 17 (from ferret 8847) containing both projection cell types, bulk loaded with OGB.

(G) Calcium responses of individual neurons were obtained using two-photon imaging while parameterized visual stimuli were presented to the animal. Two channels, one configured for visualizing OGB and one for visualizing CTB-594, were imaged simultaneously during stimulus presentation. A "functional map" was created by collapsing these two-channel images across time. For data analysis, the average time series of the OGB fluorescence within each cell, bandpass filtered to reduce slow drift and high-frequency noise, was used to obtain the cell's tuning function. Two examples of direction tuning curves are shown, one from an area 21-projecting cell (circled in blue) and one from a PSS-projecting cell (circled in red) that were imaged in the same region in response to the same stimuli. The blue trace is the mean and the gray cloud is the standard error of the response to each direction (with the preferred direction centered at 90°); the black trace is the tuning curve fitted with a harmonic model.

See also Supplemental Experimental Procedures and Figure S1.

in areas 17 and 18 were found in layers 2/3, whose depth from the cortical surface (~120–300 μm) was accessible with two-photon calcium imaging. Importantly, in most animals, it was possible to locate one or more 250 × 250 μm imaging regions containing cells projecting to each area, which allowed for within-animal comparisons between projection cell types and controlled for other factors that might affect neural responses, such as eccentricity and depth of anesthesia.

In each animal, we assigned each imaging site to either area 17 or 18 (see Figure 1A) based on its distance from the posterior pole of cortex, its overall spatial frequency preference, and its retinotopy [24, 25] (see Figure S1 and Table S1). Taken as a whole, spatial and temporal frequency preferences tended to be lower, and direction selectivity tended to be higher, in area 18 than area 17 (see Figures S2–S5). However, the differences that we observed between projection cell types were consistent within each imaging site, irrespective of its location (see Figures 2, 3, 4, and 5); thus, data from areas 17 and 18 are grouped together for statistical power in the analyses comparing the tuning preferences of cells projecting to PSS versus those of cells projecting to area 21 (comparisons are also shown separately for imaging sites in area 17 versus area 18 in the Supplemental Information). Below, when the two areas are grouped together, we refer to them as "area 17/18" [26].

Direction and Orientation Selectivity

Direction and orientation selectivity were characterized by presenting gratings whose drift direction abruptly changed by 10° each second. PSS-projecting and area 21-projecting cells were identified, and a harmonic regression model was fit to their responses to this periodic stimulus (see Supplemental Experimental Procedures and Figures S1G and S1H). Cells projecting to PSS were significantly more direction selective than cells projecting to area 21 (Figures 2A–2C), whether the cells were located in area 17 or area 18 (Figures S2A, S2B, S2D, and S2E). Calculating the direction selectivity index (DSI) of each cell using the vector average of responses in all directions, the mean and standard error of the mean of the DSI of PSS-projecting area 17/18 cells (138 cells from 13 imaging sites in 11 ferrets) was 0.25 ± 0.01, and that of area 21-projecting area 17/18 cells (113 cells from 10 imaging sites in 9 ferrets) was 0.17 ± 0.01 (t test, $p < 10^{-8}$, treating cells from all imaging sessions as independent samples). This difference was confirmed using another common method of assessing direction selectivity, by comparing the peak responses in the preferred versus nonpreferred direction: $DSI_p = (P - N)/(P + N)$, where P is the response in the preferred direction and N is the response in the nonpreferred direction. The mean DSI_p of PSS-projecting cells was 0.28 ± 0.02, and that of area 21-projecting cells was 0.16 ± 0.01 (t test, $p < 10^{-9}$). These results support the results of an electrophysiology study in macaques showing that MT-projecting cells are more strongly direction selective than the average V1 cell [27]; we extend these results to a new species using a different technique, and we directly and simultaneously compare two homologous cell types that are known to be spatially intermingled within early visual cortex but that differ in their projection targets.

The location of the injection sites and imaging chamber was consistent across animals, so that the imaged cells in areas 17

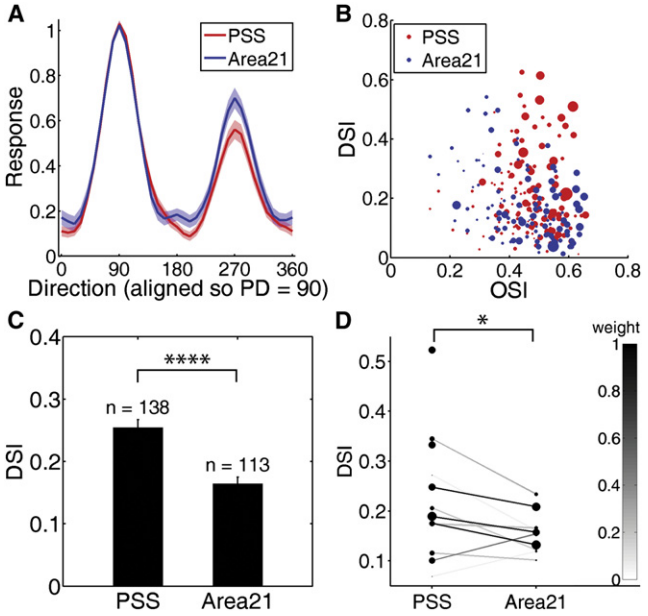

Figure 2. Direction and Orientation Selectivity

Area 17/18 cells projecting to PSS are more direction selective than area 17/18 cells projecting to area 21, but the cell groups do not differ in orientation selectivity.

(A) Weighted mean of all direction tuning curves (each cell's curve was scaled from 0 to 1 and its preferred direction was aligned at 90° before averaging). The colored shading indicates the pointwise 95% confidence interval (CI) of the weighted mean.

(B) Each cell's direction selectivity index (DSI) is plotted against its orientation selectivity index (OSI), each obtained using vector averaging (see Experimental Procedures). The size of each dot is proportional to the signal-to-noise ratio (SNR) of that cell's harmonic fit, which was used to weight the cell in the statistical analyses.

(C) Weighted mean and standard error of the weighted mean (SEM) of the DSI of each cell group. Treating all cells as independent samples, PSS-projecting cells were significantly more direction selective than area 21-projecting cells ($p < 10^{-8}$). Orientation selectivity did not differ between the two cell groups.

(D) Within-site analysis of DSI. Each "barbell" represents one imaging site; the dots without bars come from sites in which only one cell type was imaged. The size of each dot reflects the total weight contributed by that cell group in that imaging site (i.e., the number of cells × the mean weight of the cells). The darkness of each line indicates the total weight from both cell groups, which was used to weight that imaging site in a paired within-site t test (see Experimental Procedures). PSS-projecting cells were significantly more direction selective than their neighboring area 21-projecting cells ($p < 0.05$).

+0.05 < p < 0.10; *p < 0.05; **p < 0.01; ***p < 0.001; ****p < 0.001. See also Figure S2.

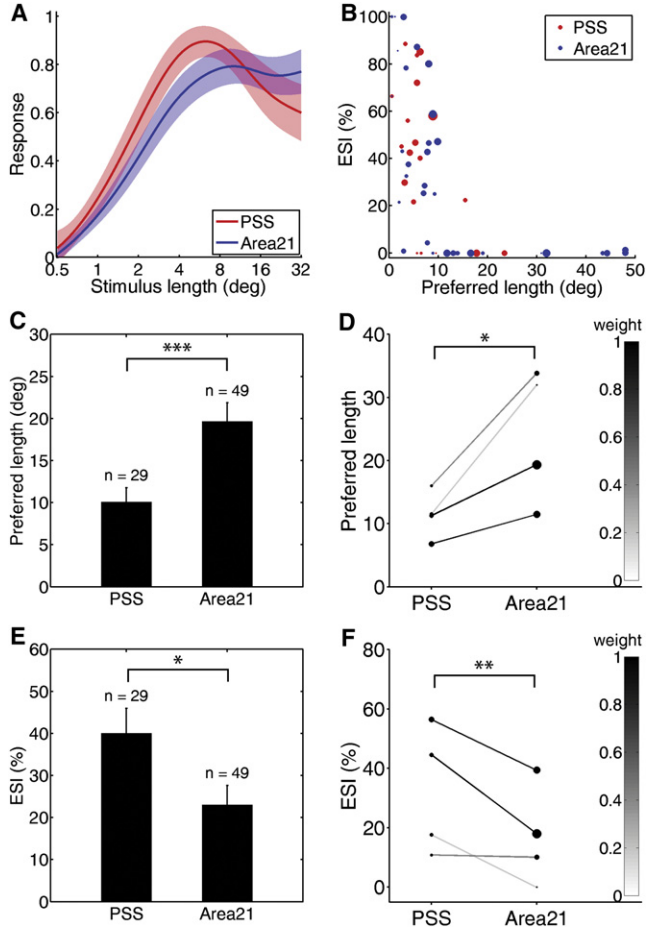

Figure 3. Length Tuning

Area 17/18 cells projecting to area 21 prefer longer stimuli than area 17/18 cells projecting to PSS.

(A) Pointwise weighted mean and 95% CI of all fitted length tuning curves.

(B) Each dot represents one cell's preferred length plotted against its end-suppression index (ESI, defined as the response to the preferred length minus the response to the longest length, as a percentage of the response to the preferred length). The size of the dot is proportional to the weight of that cell.

(C) Weighted mean and SEM of the preferred length of each cell group, treating all cells across all imaging sites as independent samples. Area 21-projecting cells had higher preferred lengths than PSS-projecting cells ($p < 0.001$).

(D) Within-site analysis of preferred length (see Figure 2 legend). Despite variability in length preferences across imaging sites, area 21-projecting cells had significantly higher preferred lengths than their neighboring PSS-projecting cells from the same imaging site ($p < 0.05$).

(E) Weighted mean and SEM of the ESI, treating all cells as independent samples. The responses of PSS-projecting cells were more strongly suppressed by long stimuli than area 21-projecting cells ($p < 0.05$).

(F) Within-site analysis of ESI, showing that this difference is also significant when comparing neighboring area 21-projecting and PSS-projecting cells ($p < 0.01$).

+0.05 < p < 0.10; *p < 0.05; **p < 0.01; ***p < 0.001; ****p < 0.001. See also Figure S3.

and 18 had similarly located receptive field eccentricity (approximately 0° to 15° azimuth and 0° to −15° elevation; see Figure S1A). Nevertheless, because tuning preferences are known to vary across the surface of areas 17 and 18 in ferrets [25] and the number of cells in one cell group was not necessarily the same as the number of cells in the other cell group at a given imaging site, it was important to control for variability in tuning properties across animals and across imaging sites. Thus, we also tested whether the observed differences between projection cell types also exist within individual imaging sites. For each imaging site in which at least one cell of each type was imaged (Figure 2D), we computed the mean DSI of the PSS-projecting cells and the mean DSI of the area 21-projecting cells and used these two DSIs as one set of data points in a paired t test. Across the ten imaging sites in which both cell types were imaged, PSS-projecting cells had a significantly higher DSI than their neighboring area 21-projecting cells ($p < 0.05$). Thus, PSS-projecting cells were more direction selective than area 21-projecting cells, even when these neurons were spatially intermingled within the same 250 × 250 μm imaging region.

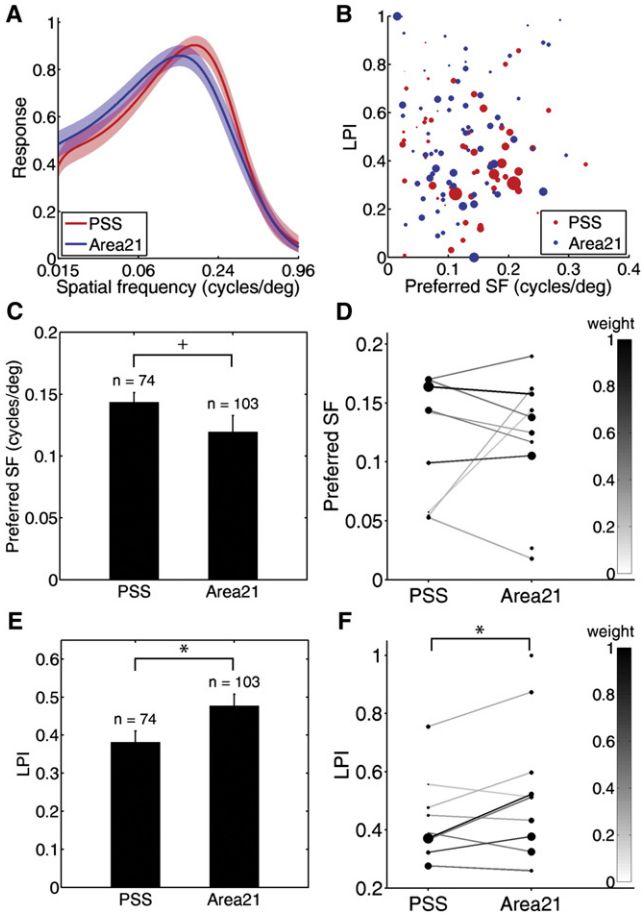

Figure 4. Spatial Frequency Tuning

Area 17/18 cells projecting to area 21 respond more strongly at low spatial frequencies (SF) than area 17/18 cells projecting to PSS.

(A) Weighted mean and 95% CI of all fitted SF tuning curves.

(B) Each dot represents one cell's preferred SF plotted against its low-pass index (LPI). The size of the dot is proportional to the weight of that cell.

(C) Weighted mean and SEM of the preferred SF of each cell group, treating all cells as independent samples. PSS-projecting cells showed a trend toward having higher preferred SF than area 21-projecting cells, though this trend did not reach significance ($p = 0.057$).

(D) Within-site analysis of preferred SF did not reveal a significant difference between cell groups imaged from the same site.

(E) Weighted mean and SEM of the LPI, treating all cells as independent samples. Area 21-projecting cells were significantly more low pass than PSS-projecting cells ($p < 0.05$).

(F) Within-site analysis of LPI. Area 21-projecting cells were significantly more low pass than their neighboring PSS-projecting cells ($p < 0.05$).

+0.05 < p < 0.10; *p < 0.05; **p < 0.01; ***p < 0.001; ****p < 0.001. See also Figure S4.

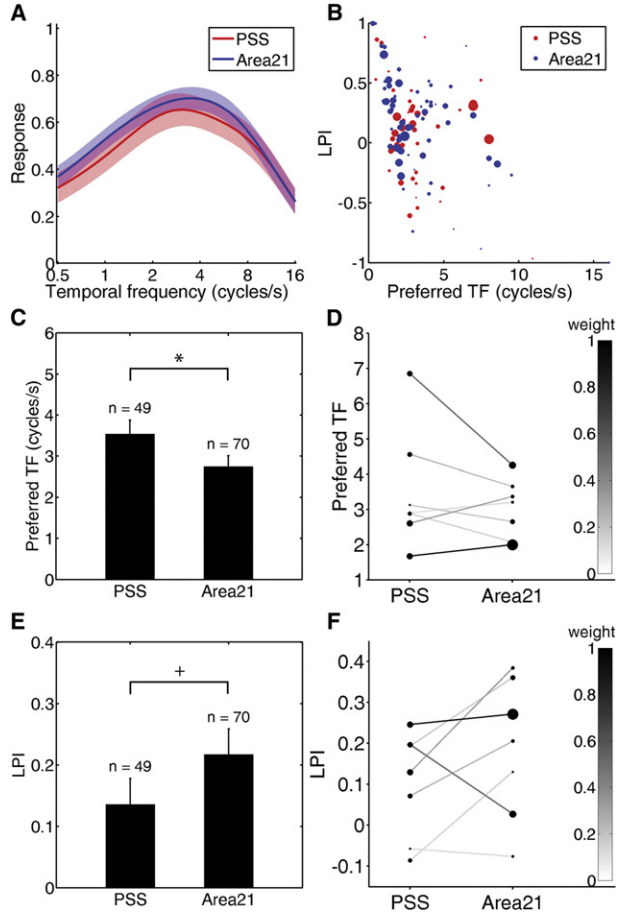

Figure 5. Temporal Frequency Tuning

Area 17/18 cells projecting to PSS prefer higher temporal frequencies (TF) than area 17/18 cells projecting to area 21.

(A) Weighted mean and 95% CI of all fitted TF tuning curves.

(B) Each dot represents one cell's preferred TF plotted against its LPI. The size of the dot is proportional to the weight of that cell.

(C) Weighted mean and SEM of the preferred TF of each cell group, treating all cells as independent samples. PSS-projecting cells preferred higher TFs than area 21-projecting cells ($p < 0.05$).

(D) Within-site analysis of preferred TF did not reveal a significant difference between cell groups imaged from the same site.

(E) Weighted mean and SEM of the LPI, treating all cells as independent samples. Area 21-projecting cells tended to be more low pass than PSS-projecting cells, though this difference did not reach significance ($p = 0.086$).

(F) Within-site analysis of LPI also did not reveal a significant difference between cell groups imaged from the same site.

+0.05 < p < 0.10; *p < 0.05; **p < 0.01; ***p < 0.001; ****p < 0.001. See also Figure S5.

PSS-projecting and area 21-projecting area 17/18 cells did not differ in their orientation selectivity (Figures 2A and 2B). The mean of the orientation selectivity index (OSI) of PSS-projecting cells was 0.50 ± 0.01, and the mean OSI of area 21-projecting cells was 0.49 ± 0.01, as measured using the vector average of responses in the 180° centered around the preferred direction. This was confirmed using another common method of assessing orientation selectivity, the half-width at half-height of the orientation tuning curve: the mean half-width at half-height for PSS-projecting cells was 36.5° ± 0.5°, and the mean for area 21-projecting cells was 35.3° ± 0.7°. These differences were also not significant.

Length Tuning

Length tuning was characterized by presenting one cycle of a grating at the optimal orientation for the imaging region and varying its length using an episodic paradigm (see Supplemental Experimental Procedures and Figures S1I and S3K). The integral of a difference of Gaussians was fit to each cell's response to the different lengths [28, 29]. The preferred length (the length at the peak of the fitted curve) and end-suppression index (ESI, the percent by which the response to the longest length is suppressed relative to the preferred length) were then obtained for each cell and compared across cell groups.

Area 17 cells projecting to area 21 preferred longer stimuli than area 17 cells projecting to PSS (Figures S3A and S3B), as

did area 18 cells (Figures S3F and S3G), and when cells in area 17 and 18 were grouped together (Figure 3), the differences in length preference between the two projection cell types were strongly statistically significant. The mean of the preferred length of area 21-projecting area 17/18 cells (29 cells from 4 imaging sites in 4 ferrets) was 19.7° ± 2.2°, and that of PSS-projecting area 17/18 cells (49 cells from the same 4 imaging sites in 4 ferrets) was 10.1° ± 1.7° (t test, $p < 0.001$, treating cells from all imaging sessions as independent samples). Additionally, the mean ESI of the area 21-projecting cells (23.0% ± 4.6%) was significantly lower than that of PSS-projecting cells (40.1% ± 5.9%; t test, $p < 0.05$). These differences in length preferences were also consistent within individual imaging sessions (Figures 3D and 3F; within-site paired t test, preferred length: $p < 0.01$; ESI: $p < 0.001$). Thus, even among area 17/18 neurons that are spatially intermingled within the same 250 × 250 μm imaging region, there are clear differences in the degree of length summation and end suppression of individual neurons that project to PSS versus to area 21.

Spatial Frequency Tuning

Spatial frequency (SF) tuning was characterized by presenting a grating at the optimal orientation and temporal frequency for the imaging region and varying its SF using an episodic paradigm (see Figures S1I and S4K). Each cell's SF tuning curve was fit to a difference of Gaussians centered at 0, representing the power spectrum of the center and surround of the receptive field [30]. The preferred SF (the SF at the peak of the fitted curve) and a low-pass index (LPI, the difference in the response to low versus high SF, normalized by the peak height) were then obtained for each cell and compared across cell groups.

Area 17/18 cells projecting to PSS had different SF preferences than area 17/18 cells projecting to area 21 (Figures 4 and S4A–S4J), though these differences were smaller than the differences in direction selectivity and length tuning. The mean of the preferred SF of PSS-projecting area 17/18 cells (74 cells from 9 imaging sites in 8 ferrets) was 0.144 ± 0.008 cycles/°, and that of area 21-projecting area 17/18 cells (103 cells from 10 imaging sites in 9 ferrets) was 0.120 ± 0.013 cycles/°. This difference in peak SF preference did not reach significance when treating all cells from all imaging sessions as independent samples, or within imaging sessions (t test, $p = 0.057$; Figure 4D). However, the area 21-projecting area 17/18 cells were slightly but significantly more low pass (LPI = 0.477 ± 0.030) than the PSS-projecting cells (0.381 ± 0.029; $p < 0.05$) when treating all cells as independent samples (Figure 4E) and within individual imaging sessions (Figure 4F; within-site paired t test, $p < 0.05$).

Temporal Frequency Tuning

Temporal frequency (TF) tuning was characterized by presenting a grating at the optimal orientation and SF for the imaging region and varying its TF using an episodic paradigm (see Figures S1I and S5K). The responses were fit to the same tuning curve model used for SF, a difference of Gaussians centered at zero, and the preferred TF and LPI were compared across cell groups.

Area 17/18 cells projecting to PSS preferred higher TFs than area 17/18 cells projecting to area 21 (Figures 5 and S5A–S5J), though these differences were also less robust than the differences in direction selectivity and length preference. The mean preferred TF of PSS-projecting area 17/18 cells (49 cells from 7 imaging sites in 6 ferrets) was 3.54 ± 0.33 cycles/s, and that of area 21-projecting area 17/18 cells (70 cells from the same imaging sites) was 2.75 ± 0.26 cycles/s (t test, $p < 0.05$, treating all cells from all imaging sessions as independent samples). The mean LPI of the PSS-projecting cells (0.136 ± 0.042) and area 21-projecting cells (0.217 ± 0.042) showed a trend in the same direction (area 21-projecting cells preferring lower TFs), but this difference did not reach significance ($p = 0.086$). The within-site differences also did not reach significance (Figures 5D and 5F).

Anatomical and Functional Clustering

To test whether the observed relationship between functional properties and anatomical projection target could be explained by overlapping patterns of functional and anatomical clustering in area 17/18, we measured for each imaging site the degree of anatomical and functional clustering and tested for a correspondence between the two (Figure 6). To test for anatomical clustering (Figures 6A–6C), same-group and different-group anatomical clustering ratios (ACRs) were compared for each imaging site containing at least two cells in each projection target group. Of the nine such imaging sites in which DSI was measured, the same-group ACRs were significantly higher than the different-group ACRs in three imaging sites (see Figure S2G for each site's p values), indicating that cells with the same projection target tended to be nearer to each other than cells with different projection targets in those three imaging sites. The imaging sites in which length, SF, and TF preference were assessed contained many of the same cells as one another and as the DSI sites, because multiple functional features were measured for each imaging site; however, the locations of the cell centers might have shifted and cells might have appeared or disappeared over time due to drift in the depth of the focal plane, so ACRs were also measured for these sites to allow for a comparison between functional and anatomical clustering within each imaging site. Of the 19 functional measure/imaging site combinations, 6 were significantly anatomically clustered (Figure S6).

To test for functional clustering in each imaging site (Figure 6D), the absolute difference in the tuning for the measured parameter in that imaging site was computed for each nearest-neighbor cell pair, and its p value was obtained by comparing the mean difference to a bootstrapped null distribution. For imaging sites in which DSI was measured, the weighted mean DSI difference among nearest neighbors was significantly lower than expected by chance in 4 of the 13 imaging sites (Figure S2G), indicating that cells nearer to each other in those imaging sites tended to have similar direction selectivity. None of the 6 imaging sites in which length preference was measured had significant functional clustering for preferred length, 4 of the 10 imaging sites in which SF was measured had significant functional clustering for preferred SF, and 1 of the 8 imaging sites in which TF was measured had significant functional clustering for preferred TF (Figure S6).

In the two imaging site/functional parameter combinations that were significant for both anatomical and functional clustering (Figures 6A and 6B), we tested for a significant correspondence between functional and anatomical clustering by comparing same-group to different-group nearest-neighbor functional differences (Figure 6E). The nearest-neighbor functional differences between cell pairs from the same anatomical group were not significantly different from the nearest-neighbor functional differences between cell pairs from different

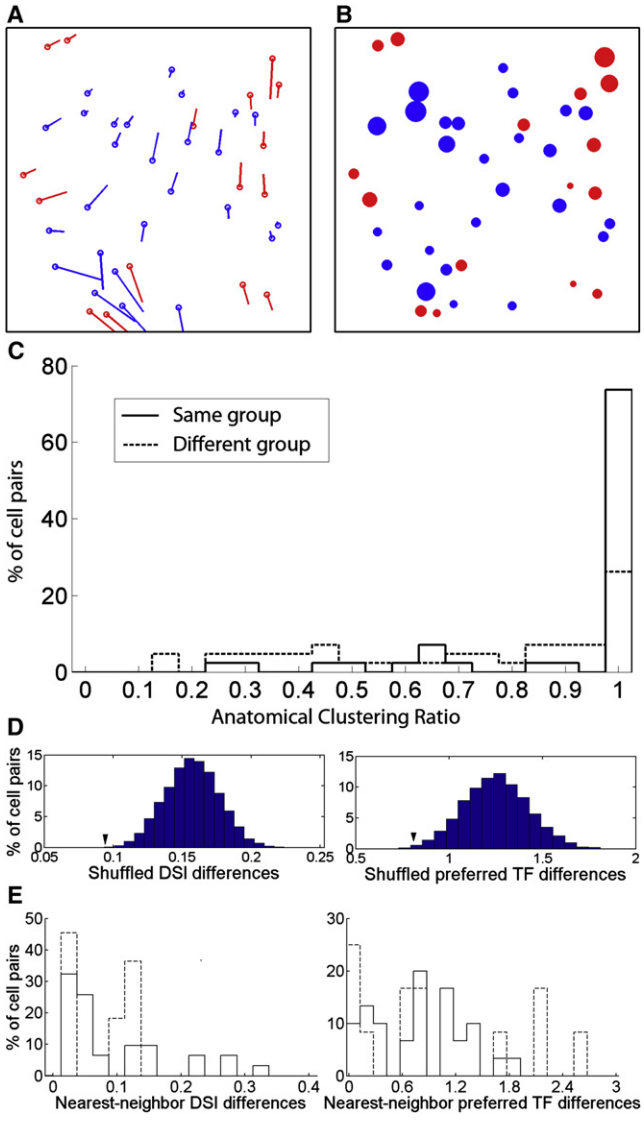

Figure 6. Functional and Anatomical Clustering

(A and B) A direction selectivity map (A) and a temporal frequency preference map (B) are shown for imaging site 8545(2), which was the only imaging site significant for both anatomical clustering and functional clustering for any functional feature. (See Figures S2G and S6 for maps of all imaging sites and all features.) The center of each cell's location in the imaging site is marked by a circle (red indicates cells projecting to PSS; blue indicates cells projecting to area 21.)

(A) Each cell's preferred motion direction is indicated by a line extending from the circle, and its relative DSI is represented by the length of the line (longer lines represent higher direction selectivity).

(B) Each cell's relative temporal frequency preference is represented by the size of the dot (larger dots represent higher preferred temporal frequency).

(C) Anatomical clustering ratio (ACR) for all nearest-neighbor cell pairs with the same (solid line) versus opposite (dashed line) projection target in this imaging site. The same-group ACRs were significantly higher than the different-group ACRs (sign test, n = 42 cells; sign = 85; Z = 3.24; $p < 0.005$), indicating that cells with the same projection target tended to be nearer to each other than cells with different projection targets.

(D) Functional clustering results. Each histogram shows the actual weighted mean of the nearest-neighbor functional differences (black arrowhead) relative to a null distribution generated by randomly shuffling the DSIs (left) or preferred TFs (right) across cells. The weighted mean DSI difference among nearest neighbors (left) was significantly lower than expected by chance ($p < 0.001$), indicating significant functional clustering in this imaging site for direction selectivity. The weighted mean TF preference among nearest neighbors (right) was also significantly lower than expected by chance ($p < 0.01$), indicating significant functional clustering for TF preference.

(E) Although this imaging site was significantly clustered both anatomically and functionally, there was no significant correspondence between its functional and anatomical clustering: the nearest-neighbor functional differences between cell pairs from the same anatomical group (solid line) were not significantly different from the nearest-neighbor functional differences between cell pairs from different anatomical groups (dashed line) (left: DSI, weighted t test, p = 0.79; right: TF, weighted t test, p = 0.65).

anatomical groups (DSI: weighted t test, p = 0.79; TF: weighted t test, p = 0.65); thus, although anatomical and functional clustering were both observed independently, there was no evidence for a correspondence between them in any imaging site.

Discussion

These results demonstrate that two populations of projection neurons that are spatially intermingled within early visual cortex have different sets of response properties that relate to the function of their respective projection targets. A previous elegant but difficult study had reported that V1 cells in macaques projecting to MT were more direction selective than the average V1 neuron by combining single-cell electrophysiological recording in V1 with antidromic stimulation in MT [27]. However, of the 745 neurons recorded in V1, only 12 were found to be antidromically activated from MT, and data were successfully collected from 9 of them. Our method provides a more powerful way to probe the relationship between anatomical connectivity and physiology simultaneously for large populations of individual neurons with known spatial relationships and multiple known projection targets.

In the present study, we found that PSS-projecting and area 21-projecting area 17/18 cells in ferrets exhibit differences in direction selectivity and stimulus length preferences, and to a lesser degree in temporal frequency preferences, that reflect the reported tuning properties of cells in their projection targets. It would be ideal to quantitatively compare the differences in tuning properties of these input cells to the tuning properties of their targets using the same methods; however, a direct comparison would be difficult because it would require recording the responses of identified pre- and postsynaptic partners. Furthermore, it is unlikely that the same stimuli could elicit robust responses in all three areas, given that tuning is known to evolve across steps in cortical processing, and in different ways along the dorsal and ventral pathways [2–4]. Although some properties of higher cortical areas are anticipated by area 17/18 responses, not all properties are equally anticipated: area 17/18 cells that project to PSS versus area 21 are most distinguished by direction selectivity, followed by length summation (or end stopping), spatial frequency selectivity, and temporal frequency selectivity. One property is seemingly anomalous: we find that PSS-projecting cells tend to prefer higher spatial frequencies than area 21-projecting cells, whereas cat PMLS cells are reported to have larger receptive fields than area 21a cells at matched receptive field eccentricity [15]. Our results therefore indicate that although biases exist in the tuning properties of cells in lower cortical areas depending on their higher-order projection targets, these input biases are further summed, amplified, and reshaped by target area circuitry [7, 8, 31].

Although we examined small (250 × 250 μm) regions of early visual cortex, we found no evidence for a correspondence between functional and anatomical clustering; i.e., in imaging regions that were significantly clustered both anatomically and functionally, neighboring cell pairs with the same projection targets did not have more similar tuning than neighboring cell pairs with different projection targets. In the absence of clustering correspondence, how might such precise, cell-specific functional-anatomical "sorting" arise?

It has been proposed that information channels originating in the retina maintain at least partial segregation through V1 into higher cortical processing streams [17, 32, 33]; however, mounting evidence argues against this possibility [34–36]. To the extent that PSS can be considered a part of the dorsal processing stream, and area 21 a part of the ventral processing stream, our findings provide further evidence against this hypothesis: the largest differences between PSS and area 21-projecting area 17/18 cells were in those functional properties that are thought to be cortically generated (direction selectivity and length preferences), not in the properties thought to be attributable to X versus Y channel inputs (spatial and temporal frequency preferences) [37, 38]. Furthermore, if we take the longer length preferences and tendency toward lower spatial frequency preferences of area 21-projecting cells as compared to PSS-projecting cells as evidence for larger receptive fields (or weaker surround inhibition), then these differences are in the opposite direction of those predicted by segregated X versus Y channel inputs.

Another possible source of the projection target-specific tuning biases in early visual cortical cells is spatially precise feedback from the higher-order areas to which they project. Indeed, well-specified functions in higher-order areas can contribute to the functional specialization of their inputs: training an artificial neural network to produce desired input-output transformations can create apparent "tuning" in the hidden layer [39, 40], and the tuning of randomly selected subsets of neurons in monkey motor cortex can be altered by changing the way their spiking activity is decoded downstream in a brain-computer interface [41]. Such feedforward-feedback interactions might play a crucial role in creating the functional biases present in the inputs to a cortical area.

The biases arising within early visual cortex might be elaborated in their target structures to generate stronger functional specialization by utilizing ubiquitous connectivity principles, similar to the way slight biases in orientation selectivity present in retinal and lateral geniculate nucleus cells [42, 43] are sharpened in V1 into strong orientation tuning by combining feedforward and recurrent inputs with the spike threshold [7–9]. Consistent with this proposal, we find that the direction selectivity of PSS-projecting area 17/18 cells is higher than area 21-projecting cells, and it is reported to be higher still within PSS [14]. Furthermore, there is evidence that biased inputs can contribute to the emergence of new computations across a single step of visual processing. For example, a large fraction of cells in monkey MT can resolve the aperture problem [44] and signal the global motion direction of a plaid pattern [45] despite the fact that V1 cells, even those projecting to MT, only signal the directions of its individual components [27, 45]; it has been proposed that global motion selectivity in MT can arise from component-selective V1 inputs if they are direction selective and end stopped [46, 47]. Here, we provide evidence supporting the mechanisms proposed in such models by showing that area 17/18 inputs to PSS (the ferret analog of MT) are indeed more direction selective and more end stopped than area 17/18 inputs to area 21 (the ferret analog of V4). The methods used here could be expanded to other sensory modalities and higher cortical areas to further support or constrain models of how new computations emerge across stages in cortical processing.

Experimental Procedures

Animals and Tracer Injection Surgery

Experiments were performed on 12 male ferrets 41–78 days old at the start of the experiment. All experimental procedures were approved by the MIT Institutional Animal Care and Use Committee and adhered to National Institutes of Health (NIH) guidelines. Pressure injections of tracer were made along the mediolateral extent of PSS (see Figure S1) and, in 10 of the 12 animals, along the mediolateral extent of area 21. PSS and area 21 were visually identified.

Two-Photon Imaging

Approximately 7 days after tracer injection, the functional properties of retrogradely labeled cells in area 17/18 were characterized using two-photon calcium imaging [48, 49]. A region in the cranial window was located that contained tracer-filled cells of both projection cell types, and two z stacks were taken from the cortical surface to 250–300 μm below the cortical surface, each with excitation and filter settings optimized for one of the tracers. Freshly prepared calcium indicator dye (Oregon green 488-BAPTA, OGB) was injected ~200 μm below the cortical surface at the chosen imaging site. Another set of z stacks was taken with an additional channel for imaging OGB, and an imaging depth was selected that contained a large number of traced cells. 256 × 256 pixel (~250 × 250 μm) images were captured from this plane at 1 Hz while visual stimuli were presented on an LCD monitor placed ~10 cm in front of the animal.

Direction and orientation selectivity

A "periodic" stimulus presentation paradigm was used for assessing direction and orientation selectivity: continuously drifting gratings were presented whose orientation and drift direction changed by 10° increments every second. Each trial consisted of three cycles around the circle, and trials were repeated 3–10 times during the course of an experiment. The drift-corrected, smoothed fluorescence time series for each cell were concatenated across trials and a tuning curve was obtained by fitting a harmonic regression model [50] (see Figures S1G and S1H). The direction selectivity index (DSI) was obtained from the fitted tuning curves using a vector average of the responses over the whole tuning curve, and separately by comparing the heights of the peaks in the preferred and nonpreferred direction (DSI_p). An orientation selectivity index (OSI) was computed using a vector average of the 180° of the direction tuning curve centered around the preferred direction, and separately as the half-width at half-height of the fitted curve.

Length, Spatial Frequency, and Temporal Frequency Tuning

An "episodic" stimulus presentation paradigm was used to assess length, spatial frequency (SF), and temporal frequency (TF) tuning. In each trial, stimulus "off" periods alternated with stimulus "on" periods in sets of four frames. In each "on" period, the parameter whose tuning function was being measured (length, SF, or TF) varied along a $\log_2$ scale while the rest of the parameters were held constant. Trials were repeated 6–10 times during the course of an experiment. Response amplitudes for each parameter value were obtained by fitting the filtered, baseline-corrected fluorescence signal with a sinusoid whose period matched the stimulus on/off cycle and whose amplitude reflected the cell's response to the stimulus (see Figure S1I), and tuning curves were obtained from these amplitudes by weighted least-squares regression to a difference of Gaussians (DoG) model for SF and TF tuning [30], or to the integral of a DoG model for length tuning [28] (see Figures S3–S5). The peaks of these tuning curves and a "low-pass index" characterizing their asymmetry around the peak were compared between cell groups.

Statistical Analysis

Instead of ignoring across-cell variability or simply discarding cells whose responsiveness to the parameter of interest did not exceed some arbitrary threshold, we weighted each cell in the statistics by its responsiveness to the parameter of interest (see Supplemental Experimental Procedures). Weighted t tests were used to compare response preferences across

groups, first treating all cells across all imaging sites as independent samples. Second, to control for factors that might affect neural responses, such as eccentricity of a given imaging site or the animal's depth of anesthesia, we also tested whether differences between cell groups existed within each imaging site: for each tuning parameter being compared, the weighted mean was obtained for each of the two cell groups in each imaging site that had at least one cell of each type. Each imaging site's pair of means was then used as one sample in a paired t test, weighting each imaging site by the total number of cells in that imaging site. Tests for anatomical and functional clustering are described in detail in Supplemental Experimental Procedures.

Supplemental Information

Supplemental Information includes six figures, one table, and Supplemental Experimental Procedures and can be found with this article online at doi:10.1016/j.cub.2012.01.011.

Acknowledgments

The authors would like to thank Amanda Mower, Beau Cronin, Ian Wickersham, Ethan Meyers, Paul Manger, Nicolas Masse, Hongbo Yu, Brandon Farley, Caroline Runyan, and Travis Emery for their contributions. This work was supported by Ruth L. Kirschstein National Research Service Award 5F32NS054390 (B.J.), NIH grants EY018648 and EY07023 (M.S.), and NIH grants DP1 OD003646 and EB006385 (E.N.B.).

Received: December 2, 2011
Revised: January 5, 2012
Accepted: January 5, 2012
Published online: February 2, 2012

References

1. Kaas, J.H. (1997). Topographic maps are fundamental to sensory processing. Brain Res. Bull. *44*, 107–112.
2. Felleman, D.J., and Van Essen, D.C. (1991). Distributed hierarchical processing in the primate cerebral cortex. Cereb. Cortex *1*, 1–47.
3. Goodale, M.A., and Milner, A.D. (1992). Separate visual pathways for perception and action. Trends Neurosci. *15*, 20–25.
4. Ungerleider, L.G., and Mishkin, M. (1982). Two cortical visual systems. In Analysis of Visual Behavior, D.J. Ingle, M.A. Goodale, and R.J.W. Mansfield, eds. (Cambridge, MA: MIT Press), pp. 549–586.
5. Lomber, S.G., Payne, B.R., Cornwell, P., and Long, K.D. (1996). Perceptual and cognitive visual functions of parietal and temporal cortices in the cat. Cereb. Cortex *6*, 673–695.
6. Payne, B.R. (1993). Evidence for visual cortical area homologs in cat and macaque monkey. Cereb. Cortex *3*, 1–25.
7. Ferster, D., and Miller, K.D. (2000). Neural mechanisms of orientation selectivity in the visual cortex. Annu. Rev. Neurosci. *23*, 441–471.
8. Somers, D.C., Nelson, S.B., and Sur, M. (1995). An emergent model of orientation selectivity in cat visual cortical simple cells. J. Neurosci. *15*, 5448–5465.
9. Sompolinsky, H., and Shapley, R. (1997). New perspectives on the mechanisms for orientation selectivity. Curr. Opin. Neurobiol. *7*, 514–522.
10. Cantone, G., Xiao, J., and Levitt, J.B. (2006). Retinotopic organization of ferret suprasylvian cortex. Vis. Neurosci. *23*, 61–77.
11. Homman-Ludiye, J., Manger, P.R., and Bourne, J.A. (2010). Immunohistochemical parcellation of the ferret (Mustela putorius) visual cortex reveals substantial homology with the cat (Felis catus). J. Comp. Neurol. *518*, 4439–4462.
12. Hupfeld, D., Distler, C., and Hoffmann, K.-P. (2007). Deficits of visual motion perception and optokinetic nystagmus after posterior suprasylvian lesions in the ferret (Mustela putorius furo). Exp. Brain Res. *182*, 509–523.
13. Hubel, D.H., and Wiesel, T.N. (1969). Visual area of the lateral suprasylvian gyrus (Clare-Bishop area) of the cat. J. Physiol. *202*, 251–260.
14. Philipp, R., Distler, C., and Hoffmann, K.P. (2006). A motion-sensitive area in ferret extrastriate visual cortex: an analysis in pigmented and albino animals. Cereb. Cortex *16*, 779–790.
15. Dreher, B., Wang, C., Turlejski, K.J., Djavadian, R.L., and Burke, W. (1996). Areas PMLS and 21a of cat visual cortex: two functionally distinct areas. Cereb. Cortex *6*, 585–599.
16. Toyama, K., Mizobe, K., Akase, E., and Kaihara, T. (1994). Neuronal responsiveness in areas 19 and 21a, and the posteromedial lateral suprasylvian cortex of the cat. Exp. Brain Res. *99*, 289–301.
17. Dreher, B. (1986). Thalamocortical and corticocortical interconnections in the cat visual system: Relation to the mechanisms of information processing. In Visual Neuroscience, J.D. Pettigrew, K.J. Sanderson, and W.R. Levick, eds. (Cambridge: Cambridge University Press), pp. 290–314.
18. Innocenti, G.M., Manger, P.R., Masiello, I., Colin, I., and Tettoni, L. (2002). Architecture and callosal connections of visual areas 17, 18, 19 and 21 in the ferret (Mustela putorius). Cereb. Cortex *12*, 411–422.
19. Manger, P.R., Kiper, D., Masiello, I., Murillo, L., Tettoni, L., Hunyadi, Z., and Innocenti, G.M. (2002). The representation of the visual field in three extrastriate areas of the ferret (Mustela putorius) and the relationship of retinotopy and field boundaries to callosal connectivity. Cereb. Cortex *12*, 423–437.
20. Morley, J.W., and Vickery, R.M. (1997). Spatial and temporal frequency selectivity of cells in area 21a of the cat. J. Physiol. *501*, 405–413.
21. Wimborne, B.M., and Henry, G.H. (1992). Response characteristics of the cells of cortical area 21a of the cat with special reference to orientation specificity. J. Physiol. *449*, 457–478.
22. Symonds, L.L., and Rosenquist, A.C. (1984). Corticocortical connections among visual areas in the cat. J. Comp. Neurol. *229*, 1–38.
23. Symonds, L.L., and Rosenquist, A.C. (1984). Laminar origins of visual corticocortical connections in the cat. J. Comp. Neurol. *229*, 39–47.
24. White, L.E., Bosking, W.H., Williams, S.M., and Fitzpatrick, D. (1999). Maps of central visual space in ferret V1 and V2 lack matching inputs from the two eyes. J. Neurosci. *19*, 7089–7099.
25. Yu, H., Farley, B.J., Jin, D.Z., and Sur, M. (2005). The coordinated mapping of visual space and response features in visual cortex. Neuron *47*, 267–280.
26. Bullier, J., Kennedy, H., and Salinger, W. (1984). Branching and laminar origin of projections between visual cortical areas in the cat. J. Comp. Neurol. *228*, 329–341.
27. Movshon, J.A., and Newsome, W.T. (1996). Visual response properties of striate cortical neurons projecting to area MT in macaque monkeys. J. Neurosci. *16*, 7733–7741.
28. DeAngelis, G.C., Freeman, R.D., and Ohzawa, I. (1994). Length and width tuning of neurons in the cat's primary visual cortex. J. Neurophysiol. *71*, 347–374.
29. Sceniak, M.P., Ringach, D.L., Hawken, M.J., and Shapley, R. (1999). Contrast's effect on spatial summation by macaque V1 neurons. Nat. Neurosci. *2*, 733–739.
30. Shapley, R., and Lennie, P. (1985). Spatial frequency analysis in the visual system. Annu. Rev. Neurosci. *8*, 547–583.
31. Douglas, R.J., and Martin, K.A. (1991). A functional microcircuit for cat visual cortex. J. Physiol. *440*, 735–769.
32. Livingstone, M.S., and Hubel, D.H. (1987). Psychophysical evidence for separate channels for the perception of form, color, movement, and depth. J. Neurosci. *7*, 3416–3468.
33. Maunsell, J.H. (1987). Physiological evidence for two visual subsystems. In Matters of Intelligence, L. Vaina, ed. (Dordrecht, Holland: Reidel), pp. 59–87.
34. Casagrande, V.A., and Royal, D. (2003). Parallel visual pathways in a dynamic system. In Primate Vision, J.H. Kaas and C.E. Collins, eds. (Boca Raton, FL: CRC Press), pp. 1–28.
35. Merigan, W.H., and Maunsell, J.H.R. (1993). How parallel are the primate visual pathways? Annu. Rev. Neurosci. *16*, 369–402.
36. Sincich, L.C., and Horton, J.C. (2005). The circuitry of V1 and V2: integration of color, form, and motion. Annu. Rev. Neurosci. *28*, 303–326.
37. Cleland, B.G., Dubin, M.W., and Levick, W.R. (1971). Sustained and transient neurones in the cat's retina and lateral geniculate nucleus. J. Physiol. *217*, 473–496.
38. Enroth-Cugell, C., and Robson, J.G. (1966). The contrast sensitivity of retinal ganglion cells of the cat. J. Physiol. *187*, 517–552.
39. Mazzoni, P., Andersen, R.A., and Jordan, M.I. (1991). A more biologically plausible learning rule than backpropagation applied to a network model of cortical area 7a. Cereb. Cortex *1*, 293–307.
40. Zipser, D., and Andersen, R.A. (1988). A back-propagation programmed network that simulates response properties of a subset of posterior parietal neurons. Nature *331*, 679–684.
41. Jarosiewicz, B., Chase, S.M., Fraser, G.W., Velliste, M., Kass, R.E., and Schwartz, A.B. (2008). Functional network reorganization during learning in a brain-computer interface paradigm. Proc. Natl. Acad. Sci. USA *105*, 19486–19491.

42. Soodak, R.E., Shapley, R.M., and Kaplan, E. (1987). Linear mechanism of orientation tuning in the retina and lateral geniculate nucleus of the cat. J. Neurophysiol. *58*, 267–275.
43. Vidyasagar, T.R., and Urbas, J.V. (1982). Orientation sensitivity of cat LGN neurones with and without inputs from visual cortical areas 17 and 18. Exp. Brain Res. *46*, 157–169.
44. Pack, C.C., and Born, R.T. (2001). Temporal dynamics of a neural solution to the aperture problem in visual area MT of macaque brain. Nature *409*, 1040–1042.
45. Movshon, J.A., Adelson, E.H., Gizzi, M.S., and Newsome, W.T. (1985). The analysis of moving visual patterns. In Experimental Brain Research Supplementum II: Pattern Recognition Mechanisms, C. Chagas, R. Gattas, and C.G. Gross, eds. (New York: Springer), pp. 117–151.
46. Beck, C., and Neumann, H. (2009). Area MT pattern motion selectivity by integrating 1D and 2D motion features from V1—a neural model. Front. Syst. Neurosci. conference abstract, Computational and Systems Neuroscience 2009. 10.3389/conf.neuro.06.2009.03.163.
47. Grossberg, S., and Mingolla, E. (1993). Neural dynamics of motion perception: direction fields, apertures, and resonant grouping. Percept. Psychophys. *53*, 243–278.
48. Schummers, J., Yu, H., and Sur, M. (2008). Tuned responses of astrocytes and their influence on hemodynamic signals in the visual cortex. Science *320*, 1638–1643.
49. Stosiek, C., Garaschuk, O., Holthoff, K., and Konnerth, A. (2003). In vivo two-photon calcium imaging of neuronal networks. Proc. Natl. Acad. Sci. USA *100*, 7319–7324.
50. Malik, W.Q., Schummers, J., Sur, M., and Brown, E.N. (2011). Denoising two-photon calcium imaging data. PLoS ONE *6*, e20490.
51. Manger, P.R., Engler, G., Moll, C.K., and Engel, A.K. (2005). The anterior ectosylvian visual area of the ferret: a homologue for an enigmatic visual cortical area of the cat? Eur. J. Neurosci. *22*, 706–714.